International Symposium
On Turbulence and Shear Flow
Phenomena (TSFP-8)
August 28 - 30, 2013 Poitiers, France

SWIRLING FLOW IN A TUBE WITH VARIABLY-SHAPED OUTLET ORIFICES: AN LES AND VLES STUDY

C.-Y. Chang, K. Dietrich, S. Jakirlic, F. Wassermann, S. Grundmann and C. Tropea
Institute of Fluid Mechanics and Aerodynamics (SLA) / Center of Smart Interfaces (CSI)
Technische Universität Darmstadt
Petersenstr. 17 D-64287 Darmstadt, Germany
chang@sla.tu-darmstadt.de, s.jakirlic@sla.tu-darmstadt.de

B. Basara
Advanced Simulation Technology, AVL List GmbH
Hans-List-Platz 1, A8020 Graz, Austria
branislav.basara@avl.com

ABSTRACT

The swirling flow in a tube with the outlet designed in the form of an orifice nozzle with centered and eccentrical openings, investigated experimentally by Grundmann *et al.* (2012), was studied computationally by employing Large Eddy Simulation (LES) method and a Hybrid LES/RANS (Reynolds-Averaged Navier-Stokes) method. The latter method, denoted by VLES (Very Large Eddy Simulation) according to Speziale (1998), represents a variable resolution computational scheme enabling a seamless transition from RANS to the direct numerical solution of the Navier-Stokes equations (DNS) depending on the ratio of the representative grid spacing to the length scale of energy containing eddies which varies within the flow domain. The background RANS model representing the basis of the VLES method is the $k-\varepsilon-\zeta-f$ model proposed by Hanjalic *et al.* (2004). The inflowing swirl generated by two tangential inlets has the same intensity in all cases considered. However, the abrupt outlet cross-section contraction created by variably-shaped orifices causes strong modification of the flow within the tube resembling a three-layered structure with alternating axial velocity directions. Both LES and VLES methods, unlike the RANS method employing the same turbulence model, returned such a behavior in good agreement with experimental data.

INTRODUCTION

The special features of swirling flows are encountered in different engineering devices. For instance a cyclone separator uses the centrifugal force arising in rotational systems to separate the solid particles from the gaseous phase. In the heat transfer application, the flow in the Ranque-Hilsch vortex tube promotes separation of the compressed gas into hot and cold streams. In combustion chambers a swirl generator is applied for the purpose of the flame stability benefiting from the swirl-induced recirculation in the combustor core. The investigations of swirl phenomena have been carried out analytically and experimentally since 1960. King *et al.* (1969) conducted the experiment of Ranque-Hilsch vortex tube for the incompressible flow and discovered the swirl decay from the initial forced vortex to free vortex at a certain distance away from the swirl generator. Gupta (1984) defined the swirl number by the ratio of tangential to axial momentum flux for the more suitable description of the swirl intensity. He also found out that the swirl number must be larger than 0.6 for the breakdown of a vortex followed by development of a transition zone. In the experimental investigation of Chang & Dhir (1994), the core and ring zones are observed, characterized by forced and free vortex. Furthermore, they pointed out to the highly anisotropic nature of the turbulent swirling flows. For the combustor configuration, the experimental investigation of Roback & Johnson (1983) represents the standard validation data for the turbulence models. Accordingly, due to the strong anisotropic feature of swirling flows, standard two equation turbulence models in the RANS framework, characterized by the scalar nature of the turbulent viscosity, fail to capture important flow properties. Reynolds stress models are inherently capable of capturing the swirling flow phenomena. Recently, the eddy resolving (ER) schemes experience growing popularity in the CFD (Computational Fluid Dynamics) community because of their enhanced sensibility towards the turbulent flow instabilities, whose correct representation is of decisive importance in the flows featured by separation and swirl.

In the present work LES, RANS and an LES-relevant eddy-resolving turbulent model named VLES are employed. The latter model provides a smooth transition from the RANS operating mode to LES depending on the grid resolution. The present VLES, based on the proposal of Speziale (1998), employs the k-ζ-f model of Hanjalic *et al.* (2004). These computational methods are validated by computing a swirling flow in a tube with variably-designed exit geometries for which the experimental reference was provided by Grundmann *et al.* (2012).

FLOW CONFIGURATION DESCRIPTION

The presently considered case is investigated experimentally by Grundmann *et al.* (2012) using Magnetic Resonance Velocimetry, providing three-dimensional and three-

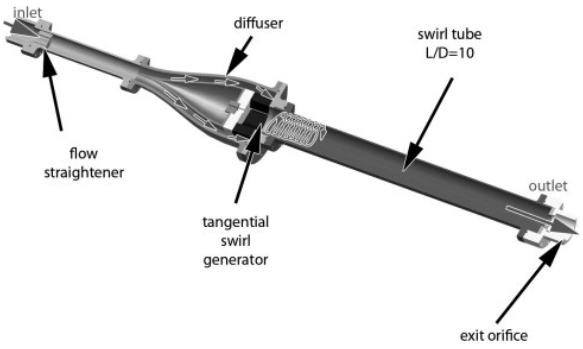

Figure 1: Flow configuration investigated presently

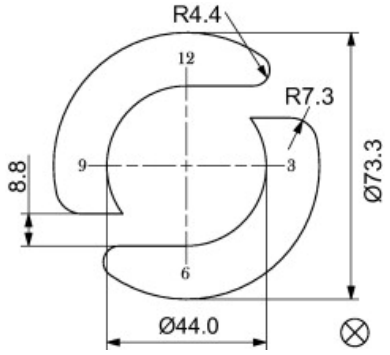

Figure 2: Cross-section of the double-tangential inlet swirl generator

component velocity distributions within entire swirl tube. The generic vortex tube with a double-tangential inlet (each having the cross sectional area of $29.33mm \times 8.8mm$) swirl generator following a ring-shaped annular diffuser, see Figs. 1 and 2. Deionized water, utilized as working medium, enters the inlet pipe (having a constant diameter of $25.4mm$ and a length of $157mm$) upstream of the diffuser. The annular diffuser supplies the swirl generator with a constant flow rate. A detailed schematic of the swirl generator is displayed in Fig. 2. The swirl tube has a length-to-diameter ratio (L/D) of 10. The tube's inner diameter (D) is $44mm$. All axial positions are denoted as the dimensionless parameter z/D, with $z/D = 0$ denoting the end of the swirl generator and $z/D = 10$ the outlet orifice location. At the end of the swirl tube, three different orifice geometries, illustrated in Fig. 3, are applied. The experiments are carried out at Reynolds number of 15000, based on the axial bulk velocity in the swirl tube, the tube diameter as characteristic length and kinematic viscosity of water at 20^oC. This corresponds to the flow rate provided by the pump of $31.05l/min$. This flow configuration, belonging to the large length-to-diameter class of the King's classification, is characterized by a strong 'circumferential' interaction between tube wall and vortex flow.

COMPUTATIONAL MODEL

The filter function-based continuity and momentum equations governing the three-dimensional, incompressible and unsteady flow read

$$\frac{\partial \widetilde{U}_i}{\partial x_i} = 0,$$

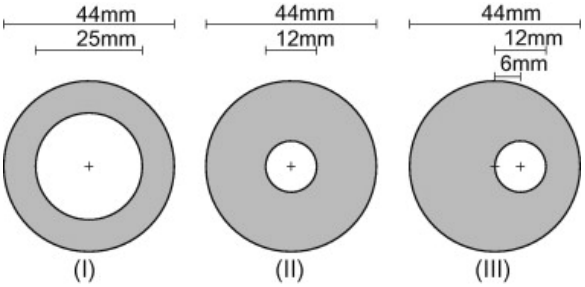

Figure 3: Variably-shaped outlet geometries: (I) large centered, (II) small centered and (III) eccentrical exit orifices

$$\frac{\partial \widetilde{U}_i}{\partial t} + \widetilde{U}_j \frac{\partial \widetilde{U}_i}{\partial x_j} = -\frac{1}{\rho}\frac{\partial \widetilde{p}}{\partial x_i} + \frac{\partial}{\partial x_j}\left(\nu \frac{\partial \widetilde{U}_i}{\partial x_j} - \widetilde{\tau}_{ij}\right) \quad (1)$$

where $\widetilde{\tau}_{ij}$ is the residual, i.e. sub-grid (SGS) stress tensor

$$\widetilde{\tau_{ij}} = \widetilde{U_i U_j} - \widetilde{U}_i \widetilde{U}_j \quad (2)$$

The rationale of the sub-grid scale eddy viscosity models is to express the residual stress tensor in terms of the resolved shear stress using Boussinesq's approximation as follows:

$$\widetilde{\tau}_{ij} = -2\nu_u \widetilde{S}_{ij} + \frac{1}{3}\widetilde{\tau}_{kk}\delta_{ij},$$
$$\widetilde{S}_{ij} = \frac{1}{2}\left(\frac{\partial \widetilde{U}_i}{\partial x_j} + \frac{\partial \widetilde{U}_j}{\partial x_i}\right) \quad (3)$$

ν_u stays here for 'unresolved' eddy-viscosity which has to be modeled.

LES. For the determination of the 'unresolved' turbulent viscosity in the LES framework, the most widely used 'standard' Smagorinsky sub-grid scale model is applied presently

$$\nu_u = (C_s\Delta)^2|\widetilde{S}_{ij}|, \quad |\widetilde{S}_{ij}| = (2\widetilde{S}_{ij}\widetilde{S}_{ij})^{\frac{1}{2}}, \quad \Delta = (\Delta_x\Delta_y\Delta_z)^{\frac{1}{3}} \quad (4)$$

here the representative mesh size Δ represents the filter width; the Smagorinsky constant C_s takes the value 0.1.

VLES. The basic principle of the VLES (Very Large Eddy Simulation) method was specified by Speziale (1998). This 'variable resolution' method employs the unsteady RANS model applying a built-in function to appropriately suppress the turbulent viscosity to the sub-grid scale level. Herewith, the RANS mode will be seamlessly bridge to LES (even to DNS with $\widetilde{\tau}_{ij} \to 0$). Following the proposal of Speziale (1998) different formulations for the built-in function were proposed in the works of Fasel *et al.* (2006), Johansen *et al.* (2004) and Han & Krajnović (2011). The presently employed VLES method utilizes the k-ζ-f model formulation ($\zeta = \overline{v^2}/k$, Hanjalic *et al.* (2004)) as the background RANS model. The model equations read as follows (here, the subscripts 'u' and 'us' indicate the (unresolved) sub-grid scale and unsteady variables respectively):

$$\frac{\partial k_{us}}{\partial t} + \widetilde{U}_j \frac{\partial k_{us}}{\partial x_j} = P_{us} - \varepsilon_{us} + \frac{\partial}{\partial x_j}\left[\left(\nu + \frac{\nu_u}{\sigma_k}\right)\frac{\partial k_{us}}{\partial x_j}\right]$$

Table 1: Constant values in the VLES-k-ζ-f model

C_μ^ζ	C_1	C_2	C_τ	C_η	C_L	σ_k	σ_ε	σ_ζ
0.22	0.4	0.65	6	50	0.36	1	1.3	1.2

$$\frac{\partial \varepsilon_{us}}{\partial t}+\widetilde{U}_j\frac{\partial \varepsilon_{us}}{\partial x_j}=\frac{C_{\varepsilon_1}P_{us}-C_{\varepsilon_2}\varepsilon_{us}}{T_{us}}+\frac{\partial}{\partial x_j}\left[\left(\nu+\frac{\nu_u}{\sigma_\varepsilon}\right)\frac{\partial \varepsilon_{us}}{\partial x_j}\right]$$
$$\frac{\partial \zeta_{us}}{\partial t}+\widetilde{U}_j\frac{\partial \zeta_{us}}{\partial x_j}=f_{us}-\frac{P_{us}}{k_{us}}\zeta_{us}+\frac{\partial}{\partial x_j}\left[\left(\nu+\frac{\nu_u}{\sigma_\zeta}\right)\frac{\partial \zeta_{us}}{\partial x_j}\right]$$
$$L_{us}^2\nabla^2 f_{us}-f_{us}=\frac{1}{T_{us}}\left(C_1+C_2\frac{P_{us}}{\varepsilon_{us}}\right)\left(\zeta_{us}-\frac{2}{3}\right) \quad (5)$$

The unsteady turbulent time scale and length scale switches are defined as follows:

$$T_{us}=\max\left[\frac{k_{us}}{\varepsilon_{us}},C_\tau\left(\frac{\nu}{\varepsilon_{us}}\right)^{\frac{1}{2}}\right],\ L_{us}=\max\left[\frac{k_{us}^{1.5}}{\varepsilon_{us}},C_\eta\left(\frac{\nu^3}{\varepsilon_{us}}\right)^{\frac{1}{4}}\right] \quad (6)$$

The corresponding sub-grid scale turbulent viscosity is defined as

$$\nu_u=F_r C_\mu^\zeta \zeta_{us}k_{us}T_{us} \quad (7)$$

with the built-in function taking the following form

$$F_r=\min\left[\left(\frac{\Delta}{\Lambda_{us}}\right)^{\frac{4}{3}},1\right],\quad \Lambda_{us}=\frac{(k_{us})^{\frac{3}{2}}}{\varepsilon_{us}}. \quad (8)$$

The VLES suppresses the modeling level in an explicit manner depending on the grid spacing. By assuming the total dissipation rate corresponding to the unsteady mode according to the Kolmogorov's hypothesis, the relation between sub-grid scale turbulent kinetic energy (k_u) and modeled unsteady kinetic energy (k_{us}) becomes:

$$k_u=F_r^{\frac{1}{2}}k_{us}=\left(\frac{\Delta}{\Lambda_{us}}\right)^{\frac{2}{3}}k_{us}. \quad (9)$$

The present VLES method is preliminary validated in the naturally decayed homogeneous isotropic flow (not shown here), flow in a plane channel and a separating flow over a periodic arrangement of 2D hills. The initial fields in the latter two cases correspond to the steady RANS results. The plane channel flow was meshed by $(N_x,N_y,N_z)=(64,100,64)$ grid cells. The profiles of the mean velocity and all Reynolds stress components exhibit a very good agreement with the DNS results of Moser *et al.* (1999), Figs. 4. The flow over a 2D hill at $Re=10600$ (reference LES by Froehlich *et al.* (2005) and experiment by Rapp & Manhart (2011)) was computed by using the mesh comprising only $(80\times100\times30)$ grid cells. Fig. 5 displays the vorticity contours illustrating the instantaneous flow field obtained. The turbulence activity in the separated shear layer especially in the region of separation is appropriately enhanced compared to the outcome of the background RANS model resulting finally in the correct prediction of the recirculation zone size (see the friction factor development), Figs. 6.

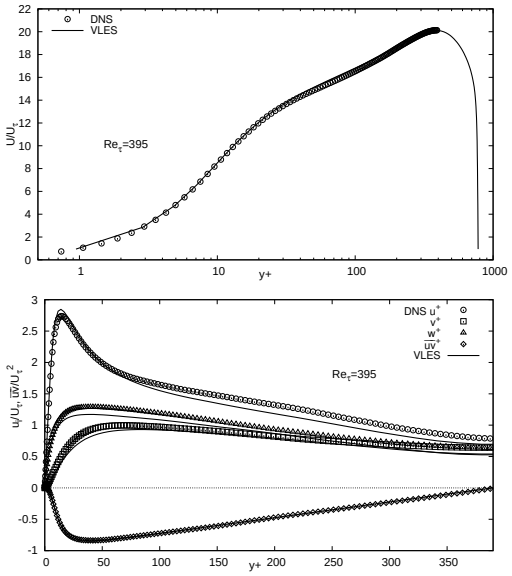

Figure 4: Channel flow at $Re_\tau=395$, mean velocity and Reynolds stress component profiles

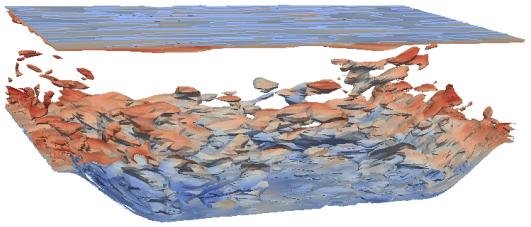

Figure 5: Flow over a 2D hill, vorticity magnitude

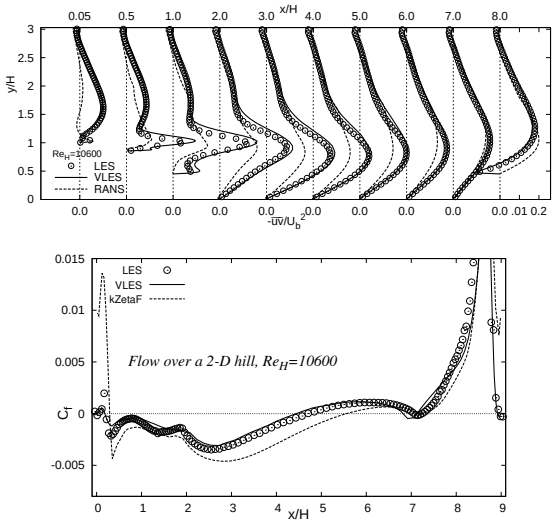

Figure 6: Flow over a 2D hill, shear stress component and friction factor developments

NUMERICAL METHOD

All computations were performed using the commercial CFD software package AVL FIRE v2011. The code employs the finite volume discretization method, which rests on the integral form of general conservation law applied to the polyhedral control volume. All dependent variables are stored at the geometric center of the control

volume. The appropriate data structure and interpolation practices for gradients and cell-face values are introduced to accommodate an arbitrary number of cell faces. The convection can be approximated by variety of differencing schemes. The diffusion is approximated using central differencing. The overall solution procedure is iterative and is based on the SIMPLE algorithm, which ensure coupling between the velocity and pressure fields. The filter-based hybrid models are presently applied in conjunction with the universal wall treatment. This method blends the integration up to the wall boundary conditions with the wall functions, enabling well-defined boundary conditions irrespective of the position of the wall-closest computational node. Popovac & Hanjalic (2007) proposed the so-called compound wall treatment with a blending formula for the quantity specified at the central node P of the wall-closest grid cell as $\phi_P = \phi_v e^{-\Gamma} + \phi_t e^{-1/\Gamma}$, where v denotes the viscous and t the fully turbulent values. The variable ϕ relates to the wall shear stress, production and dissipation of the turbulent kinetic energy. A somewhat modified approach was implemented into the CFD software AVL FIRE, Basara et al. (SAE Technical Paper Series, Paper No. 2007-01-0104).

COMPUTATIONAL DETAILS

The computational domain is configured as a simplified geometry compared to the experimental setup with two tangential duct inlets connected to the swirl tube. Fixed mass flow value of $0.258 kg/s$ is prescribed at each inlet; zero-gradient boundary condition is applied at the outlet plane. Each inlet duct is meshed by $(25 \times 20 \times 40)$ cells in streamwise, normal and spanwise directions. The whole domain is meshed by around 1.2 million hexahedral cells with 160 cells in axial direction, Fig. 7. Between the inlet duct and cylinder, appropriate interpolation is applied to avoid too high aspect ratio of the cells. The maximum y^+-values at the tube wall is less than 7. The quality of the mesh resolution within the computational domain is illustrated by the ratio of the representative grid spacing to the Kolmogorov length scale Δ/η, exhibiting its maximum in the immediate tube wall vicinity where this ratio amounts to ≈ 40, Fig. 7. In the largest portion of the solution domain this value is well under 15, even under 5 in the flow core. Further insight into the suitability of the mesh resolution applied can be gained by displaying the level of the modeled (unresolved) turbulent viscosity, Fig. 8. Whereas the ratio ν_u/ν corresponding to the LES simulation doesn't exceed the value of 3, the relevant value corresponding to VLES simulation is less than 7. The exception is very narrow region around the outlet orifice where the values about 13 are documented. The distribution of the transition, built-in function is depicted in Fig. 9. With exception of the wall proximity of the pipe inflow region, where $F_r \approx 1$, indicating the RANS operation mode of the VLES method, this parameter takes the values around 0.1 in the largest portion of the flow domain. Details corresponding to all three investigated geometries are listed in Table 2. The mean flow and turbulent statistics is obtained after averaging for 5 seconds of physical flow time after reaching the fully-developed turbulent state.

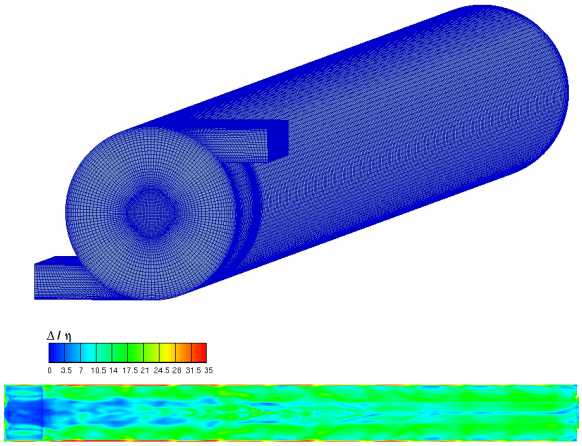

Figure 7: Swirl tube with large centered exit orifice - numerical mesh and Δ/η distribution

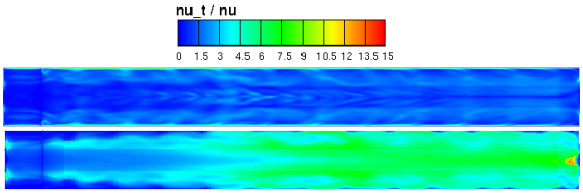

Figure 8: Large centered exit orifice - modeled fraction levels illustrated by the ratio (ν_u/ν) obtained by LES (upper) and VLES (lower)

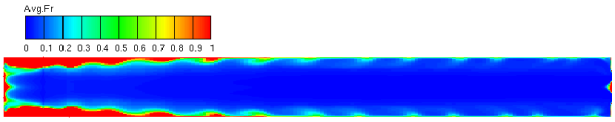

Figure 9: Large centered exit orifice - distribution of the parameter F_r

Table 2: Computational details

Exit orifice type	Large centered	Small centered	Eccentrical
No. of cells	1197768	1267272	1294920
max. Δ/η	42.11	41.77	41.36
max. y^+	4.71	6.32	6.27

RESULTS AND DISCUSSION

Selected results obtained by applying all three presently considered computational methods (LES, RANS and VLES) to three flow configurations characterized by differently shaped exit orifice are displayed in Figs. 10-16 (the results related to the large centered exit orifice are not shown here due to sake of brevity). First impression about the flow structure can be obtained from Fig. 10 displaying the instantaneous axial velocity field. The alternation

of the flow direction across the pipe indicating a three layered structure in the axial velocity distribution induced by swirl in combination with the outlet cross-section contraction is obvious. A fluid jet with high axial velocity develops along the tube's centerline, denoted as core jet. This phenomenon is surrounded by a recirculation zone with negative axial velocity. The majority of mass flow rate is moved through the ring zone, in which low-intensity left-handed helical structures of high axial velocity, termed wall jets, could be visualized. In the core region a solid body vortex occurs, whereas a potential vortex exists in the recirculation and ring zones, Figs. 11-16. This is observed qualitatively in all three cases investigated, the differences are related mostly to the intensity of the core jet and flow recirculation.

Grundmann *et al.* (2012) observed in their experimental work some interesting flow features, see Fig. 13 and Fig. 16. In the axial flow direction, the intensity of core jet increases towards the outlet orifice. Regarding the helical structure in the geometries characterized by the centered exit orifice shape, the ring zone and corresponding streamlines are both oriented towards the left-handed direction, in line with the direction originating from the swirl generator, Fig. 13. An interesting phenomenon appears in the configuration with eccentrical exit orifice: the streamlines show towards the left-handed direction, as in the centered orifice cases, but, due to the outlet eccentricity, the helical structures in the ring zone experience an opposite orientation towards the right-handed direction, see Fig. 16. This feature is well captured by LES and VLES.

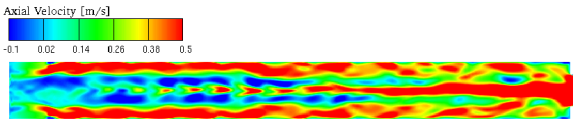

Figure 10: Swirl tube with large centered exit orifice - instantaneous axial velocity field

Quantitatively, the intensity of the core jet along the vortex tube is somewhat underestimated by LES and VLES. The concentrated vortex shape of the tangential velocity field is correctly returned by both eddy-resolving methods, LES and VLES; this is especially the case for the LES simulation. As expected, the circumferential velocity field computed by the RANS method employing the $k-\zeta-f$ model exhibits a solid body profile shape being typical of the eddy-viscosity modeling group due to the scalar nature of the turbulent viscosity.

CONCLUSIONS

An eddy resolving model based on the grid filter function, denoted by VLES, is formulated using the $k-\zeta-f$ model as the background RANS model. Both model versions, together with the conventional LES method utilizing the standard Smagorinsky SGS model, are applied to a flow in a swirling pipe with differently designed exit geometry concerning the shape of centered and eccentrical orifices. Such a constellation induces a very interesting three-layered structure (core jet, recirculation and ring zone) characterizing the axial velocity distribution and a two-layered structure (solid-body vortex and potential vortex) of the tangential velocity field. Especially interesting is the helical structure in the ring zone of the pipe corresponding to the eccentrical case being oriented contrary to the swirling flow issuing from the swirl generator. Both LES and VLES returned this phenomenon qualitatively correctly, unlike the eddy-viscosity-based RANS-$k-\zeta-f$ model.

REFERENCES

Chang, F. & Dhir, V.K. 1994 Turbulent-flow field in tangentially injected swirl flows in tubes. *Int. J. Heat and Fuid Flow* **15** (5), 346–356.

Fasel, H.F., von Terzi, D.A. & Sandberg, R.D. 2006 A methodology for simulating compressible turbulent flows. *ASME J. App. Mech.* **73** (3), 405–412, .

Froehlich, J., Mellen, C.P., Rodi, W., Temmerman, L. & Leschziner, M.A. 2005 Highly resolved large-eddy simulation of separated flow in a channel with streamwise periodic constrictions. *J. Fluid Mech.* **526**, 19–66.

Grundmann, S., Wassermann, F., Lorenz, R., Jung, B. & Tropea, C. 2012 Experimental investigation of helical structures in swirling flows. *Int. J. Heat and Fluid Flow* **37**, 51–63.

Gupta, Ashwani K 1984 *Swirl flows*. Technomic Publishing Co., Lancaster, PA.

Han, X. & Krajnović, S. 2011 A new very large eddy simulation model for simulation of turbulent flow. *Advances in Hybrid RANS-LES Modelling 4, Notes on Numerical Fluid Mechanics and Multidisciplinary Design* **117**, 131–140, Springer Verlag (ISBN 978–3–642–31817–7).

Hanjalic, K., Popovac, M. & Hadziabdic, M. 2004 A robust near-wall elliptic-relaxation eddy-viscosity turbulence model for CFD. *Int. J. Heat and Fluid Flow* **25** (6), 1047–1051.

Johansen, S.T., Wu, J.Y. & Shyy, W. 2004 Filter-based unsteady RANS computations. *Int. J. Heat and Fluid Flow* **25** (1), 10–21.

King, M.K., Rothfus, R R. & Kermode, R.I. 1969 Static pressure and velocity profiles in swirling incompressible tube flow. *AIChE Journal* **15** (6), 837–842.

Moser, R.D., Kim, J. & Mansour, N.N. 1999 Direct numerical simulation of turbulent channel flow up to $re_\tau = 590$. *Physics of fluids* **11**, 943.

Popovac, M. & Hanjalic, K. 2007 Compound wall treatment for rans computation of complex turbulent flows and heat transfer. *Flow, Turbulence and Combustion* **78** (2), 177–202.

Rapp, Ch. & Manhart, M. 2011 Flow over periodic hills: an experimental study. *Exp. in Fluids* **51**, 247–269.

Roback, R. & Johnson, B. V. 1983 Mass and momentum turbulent transport experiments with confined swirling coaxial jets. *Tech. Rep.*. .

Speziale, CG 1998 Turbulence modeling for time-dependent RANS and VLES: A review. *AIAA J.* **36** (2), 173–184, .

ACKNOWLEDGEMENT

The financial support of the company AVL List GmbH, Graz, Austria is gratefully acknowledged.

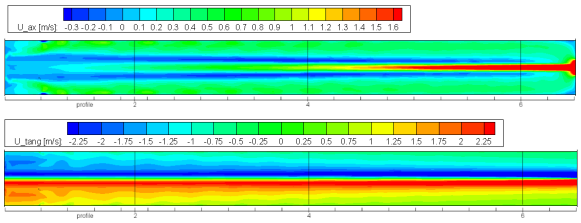

Figure 11: Small centered exit orifice - axial (upper) and tangential (lower) velocity contours obtained by LES

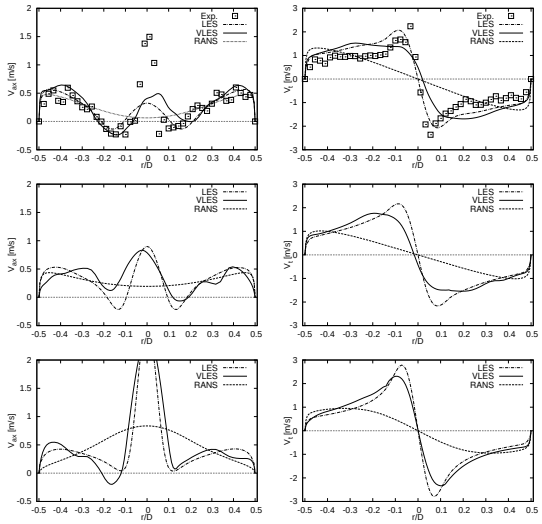

Figure 12: Small centered exit orifice - axial (left) and tangential (right) velocity profiles at $z/D = 1.75(upper), 5(middle), 9(lower)$

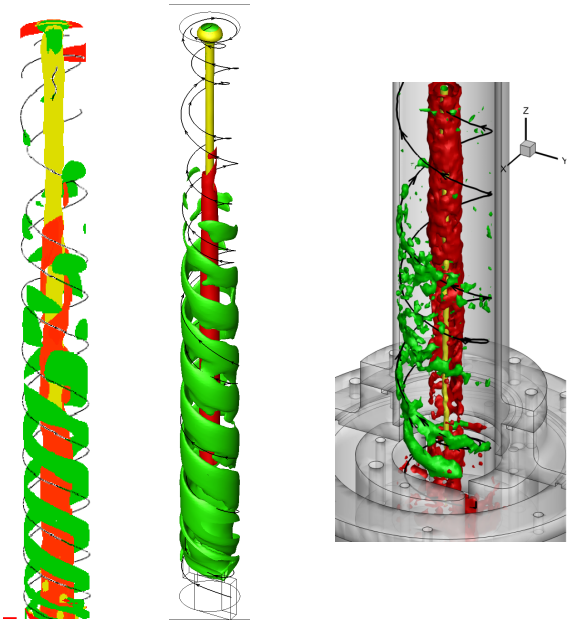

Figure 13: Small centered exit orifice - iso-contours of the axial velocity field obtained experimentally (right), by VLES (left) and LES (middle)

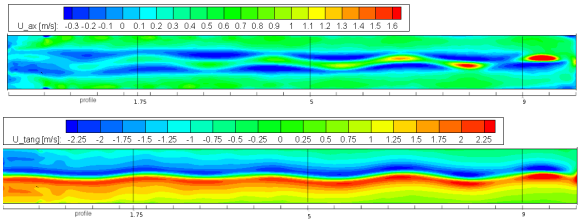

Figure 14: Eccentrical exit orifice - axial (upper) and tangential (lower) velocity contours obtained by LES

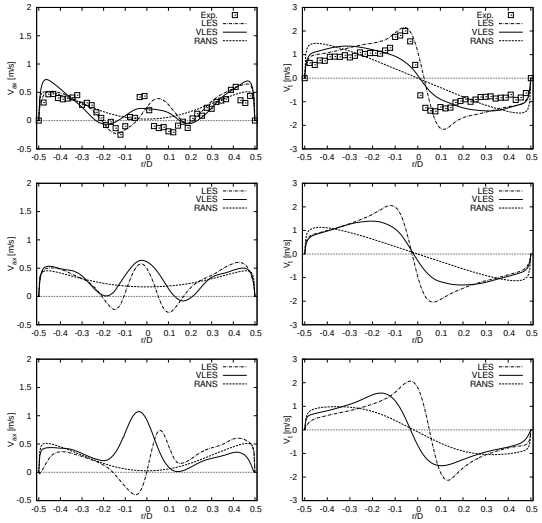

Figure 15: Eccentrical exit orifice - axial (left) and tangential (right) velocity profiles at $z/D = 1.75(upper), 5(middle), 9(lower)$

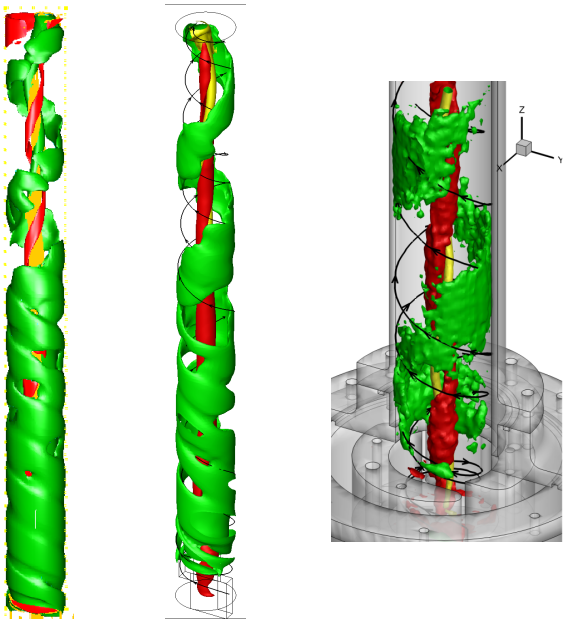

Figure 16: Eccentrical exit orifice - iso-contours of the axial velocity field obtained experimentally (right), by VLES (left) and LES (middle)